Drug likeness prediction of 5-hydroxy-substituted coumarins with high affinity to 5-HT1A and 5-HT2A receptors

Teresa Żołek, Éva A. Enyedy, Kinga Ostrowska, Vivien Pósa, Dorota Maciejewska

PII: S0928-0987(18)30018-6
DOI: https://doi.org/10.1016/j.ejps.2018.01.011
Reference: PHASCI 4361

To appear in: *European Journal of Pharmaceutical Sciences*

Received date: 2 November 2017
Revised date: 28 December 2017
Accepted date: 4 January 2018

Please cite this article as: Teresa Żołek, Éva A. Enyedy, Kinga Ostrowska, Vivien Pósa, Dorota Maciejewska , Drug likeness prediction of 5-hydroxy-substituted coumarins with high affinity to 5-HT1A and 5-HT2A receptors. The address for the corresponding author was captured as affiliation for all authors. Please check if appropriate. Phasci(2017), https://doi.org/10.1016/j.ejps.2018.01.011

Drug likeness prediction of 5-hydroxy-substituted coumarins with high affinity to 5-HT_{1A} and 5-HT_{2A} receptors

Teresa Żołek,[a] Éva A. Enyedy,[b] Kinga Ostrowska,[a] Vivien Pósa,[b] and Dorota Maciejewska[a]*

[a] Department of Organic Chemistry, Faculty of Pharmacy, Medical University of Warsaw, Banacha 1, 02-097 Warsaw, Poland

[b] Department of Inorganic and Analytical Chemistry, University of Szeged, Dóm tér 7. H-6720 Szeged, Hungary

*Corresponding Author: Phone/Fax: (+48)-022-5720643 E-mail address: dmaciejewska@wum.edu.pl (prof. D. Maciejewska)

ABSTRACT

One of the latest trends is search for the new anti-psychotic drugs among coumarin derivatives with piperazine moiety. Their therapeutic potential can be hampered by poor physico-chemical parameters as low brain penetration or limited transport in the body fluid. Herein, we predicted the drug likeness of six coumarins with high affinity towards 5-HT_{1A} and 5-HT_{2A} receptors. Subsequent experimental determination of their binding constants to human serum albumin (HSA) revealed the binding with a moderate strength (logK = 4.8 – 5.8) at the Sudlow's site 1, which represents a possibility of temporary storage of tested coumarins on HSA. Computational mapping of the binding of coumarins - HSA complexes showed that the coumarin rings of all tested compounds were similarly located within the hydrophobic binding pocket of HSA, while the rest of molecules (composed with alkyl chains, piperazine and benzene rings)

decided about the difference in binding modes by the hydrogen bonding interactions. The proton dissociation constants (pK_a) of the compounds were also determined by UV–vis spectrophotometric titrations to obtain the distribution of the species in the different protonation states at physiological pH of 7.4. A good agreement of the computationally-determined free enthalpy values of the ligand – HSA complexes with the values determined by experimental fluorescence quenching data could be a promising prospect for proposed theoretical strategy.

Keywords: 5-hydroxycoumarins; drug likeness parameters; human serum albumin binding; fluorometry; molecular simulations; proton dissociation constants.

1. Introduction

The clinical potential of drugs is greatly affected by the nature of their interactions with circulating plasma proteins, such as human serum albumin (HSA), α_1-acid glycoprotein, lipoproteins and α-, β-, γ-globulins (Bailey and Briggs, 2004; Bertucci and Domenici, 2002; Peters, 1996). Plasma protein binding can impact on the free concentration of drug in the circulation, the distribution around the body and the duration of drug action. It is generally accepted that the bound or the unbound drug molecules in blood plasma are in equilibrium, but only the unbound quantity of drug is pharmacologically active and able to pass through cell membranes (Flarakos et al., 2005). Thus, it is important to determine the fraction of unbound drugs at various stages of drug development, and during ADMET (absorption, distribution, metabolism, elimination and toxicity) parameters studies (Hogson, 2001). There is also a strong correspondence between interactions of drug candidate with plasma proteins and its pathways inside the human body, therefore computational evaluation of protein-drug energies can help in

the characterization of problems generated by protein binding (Ahmed-Ouameur et al., 2006; Curry, 2009; Flarakos et al., 2005).

Among the plasma proteins, HSA is the most important transporter for endogenous (fatty acids, hormones, bile acids, amino acids, etc.) and exogenous compounds (therapeutic drugs and nutrients) (Bhattacharya et al., 2000; Ghuman et al., 2005; Petitpas et al., 2003), because of its relatively high concentration with respect to other plasma proteins (Pérez-Ruiz et al., 2010; Peters, 1996). The binding modes are encoded in the secondary structure of HSA which is an α-helix single-chain protein formed by three homologous domains (I, II and III) with each domain divided into subdomains A and B. Although many binding sites have been reported for ligands in HSA, the most important sites are commonly known as Sudlow´s sites 1 and 2 which are found in subdomains IIA and IIIA, respectively (Sudlow et al., 1976; Varshney et al., 2010). According to crystallographic studies ligands such as fatty acids can bind up to seven sites in HSA including both Sudlow´s sites (Carter and Xo, 1994). Site 1 is a large, flexible and multi-chamber cavity within the core of subdomain IIA that comprises all six helices of the subdomain and additional residues from subdomains IB, IIB and IIIA (Ryan et al., 2011). Site 2 in subdomain IIIA is smaller than site 1, and is a largely apolar cavity with well-defined polar features. This site appears to be less flexible, since ligand binding to this site often shows stereoselectivity, and binding is strongly affected by small structural modifications of the ligand (Ghuman et al., 2005). Most of compounds used in human therapy bind to these two sites with affinities constants (K) of 10^4 – 10^6 M^{-1} (Kratochwil et al., 2002). The ligand interaction with HSA can be probed by changes of fluorescence emission which is due to the presence of the single tryptophan residue (Trp-214) located in the subdomain IIA of site 1 (Il'ichev et al., 2002; Petitpas et al., 2001).

In recent years, various research groups have been involved in the examinations of conformational changes of HSA, joined with the interaction between protein and biologically active natural and synthetic compounds such as coumarin and its analogues (Dömötör et al., 2014; Garg et al., 2013; Gokara et al., 2010; Yeggoni et al., 2014). The potency of coumarins may be modified by the number of small substituents, such as the hydroxy, alkoxy or carbonyl groups in various positions of coumarin moiety (Abdelhafez et al., 2010; Drzewiecka et al., 2013; Hassan et al., 2016; Paul et al., 2013; Sarkanj et al., 2013; Tsay et al., 2013). One of the latest trends is search for the new anti-psychotic drugs among coumarin derivatives, and their affinities to serotoninergic receptors 5-HT_{1A} and 5-HT_{2A} were defined (Chen et al., 2014; Chen et al., 2013). Several studies have shown that activation of 5-HT_{1A} receptor increases dopamine release in the frontal cortex, which may improve negative symptoms and cognitive deficits in schizophrenia (Lameh et al., 2007). Thus, coumarins are a potential resource of compounds for the prevention and therapy of selected central nervous system (CNS) diseases (e.g. anxiety, depression, schizophrenia, Alzheimer´s and Parkinson´s disease) (Skalicka-Wozniak et al., 2016).

In this study we selected six compounds synthesized in our research group which belong to 5-hydroxycoumarin family connected with the *N*-arylpiperazine substituent via propyloxy or butyloxy linkers. These compounds revealed in *in vitro* assays very high affinities to 5-HT_{1A} (IC_{50} within range 0.3 – 1.0 nM) and high affinities to 5-HT_{2A} (IC_{50} within range 9.0 – 184.0 nM) receptors (Ostrowska et al., 2017). As the next step in the pipeline of drug discovery are *in vivo* tests, we calculated the theoretical values of the physico-chemical and biopharmaceutical parameters which describe the absorption, distribution, metabolism, elimination and toxicity (ADMET) in the human body to select the best candidates to these examinations. All compounds

were predicted to bind to blood plasma proteins. Then, we used the combination of experimental and computational techniques to understand and characterize the interactions of tested compounds with a major carrier protein HSA using fluorescence spectroscopic technique, molecular docking and molecular dynamics (MD) simulations.

2. Theoretical methodology

2.1. Theoretical structures of protein and ligands

We tested six compounds: 6-acetyl-4,7-dimethyl-5-[3-(4-(2,3-dichlorophenyl)piperazin-1-yl)propoxy]coumarin (**1**), 6-acetyl-4,7-dimethyl-5-[3-(4-(2-fluorophenyl)piperazin-1-yl)propoxy]coumarin (**2**), 6-acetyl-4,7-dimethyl-5-[3-(4-(3-methoxyphenyl)piperazin-1-yl)propoxy]coumarin (**3**), 6-acetyl-4,7-dimethyl-5-[3-(4-(2-cyanophenyl)piperazin-1-yl)propoxy]coumarin (**4**), 6-acetyl-4,7-dimethyl-5-[4-(4-(2-fluorophenyl)piperazin-1-yl)butoxy]coumarin (**5**) and 4,7-dimethyl-5-[4-(4-(3-methoxyphenyl)piperazin-1-yl)butoxy]coumarin (**6**) (Fig. 1) which showed the highest affinity towards 5-HT_{1A} and 5-HT_{2A} receptors. They belong to two groups of coumarin derivatives, which differ in the length of the linker between the coumarin and the piperidine rings: compounds **1** – **4** have propylene and compounds **5** – **6** have butylene chains. Coumarin derivatives are poorly soluble in water, and prior to biological tests they were transformed into hydrochlorides to increase solubility. For consistency sake we analyzed the cations of **1** – **6** in the theoretical studies. Three-dimensional structures of ligands were prepared using Discovery Studio 4.5 visual interface BIOVIA (Biovia Software Inc., 2015). Geometries of all compounds were optimized using the density functional theory (DFT) with the B3LYP/6-311G (d,p) hybrid functional, as implemented in Gaussian 09 (Frish et al., 2009). ESP-atomic partial charges on all atoms were computed using the Breneman

model reproducing the molecular electrostatic potential (Breneman and Wiberg, 1990). The structures were then exported into the 3D SDF format and used as input in ADMET Predictor^{TM} version 8.0 (Simulations Plus Inc.) software to calculate the values of molecular descriptors by the mathematical models. The crystal structure of HSA (PDB ID: 2BXD) was obtained from the RCSB Protein Data Bank. The PDB file presents a co-crystal with a warfarin ligand in the active site. Ligand, water molecules and inorganic ions were removed prior to the calculations and hydrogen atoms were added to reflect the physiological pH.

2.2. Prediction of drug likeness descriptors and toxicity

The molecular descriptor values of compounds **1** – **6** were used as inputs to mathematical models implemented in ADMET Predictor^{TM} version 8.0 in order to generate estimates for each of the ADMET property. In this study we checked Lipinski's rule of five and then we calculated the following descriptors: the topological polar surface area (TPSA), distribution coefficient logD (at pH = 7.4), the volume of distribution (V_d), the solubility (S_w), the proton dissociation constants (pK_a), Madin-Darby Canine Kidney cells apparent permeability (MDCK), the effective permeability (P_{eff}), the blood-brain BBB filter, the blood-brain barrier (BBB) partition coefficient $logC_{brain}/C_{blood}$ (logBB), percentage of unbound drug to proteins within blood plasma (%Unbnd) and blood-to-plasma concentration ratio (RBP = $C_{whole\text{-}blood}/C_{plasma}$). Toxicity profile was characterized by Maximum Recommended Therapeutic Dose (MRTD), cardiac toxicity by affinity towards hERG-encoded potassium channels, and the hepatotoxicity (described by the level of alkaline phosphatase (AlkPhos), γ-glutamyl transferase (GGT), serum glutamate oxaloacetate transaminase (SGOT), serum glutamate pyruvate transaminase (SGPT) and lactate dehydrogenase (LDH)).

2.3. HSA-ligand docking study

Docking was performed using AutoDock 4.2.3 software (Morris et al., 2009), and the Lamarckian Genetic Algorithm (LGA) (Morris et al., 1998), since it was found to be the best performing docking method in terms of its ability to find the lowest energy (Morris et al., 1996; Morris et al., 2009). The protein input files were prepared for docking by adding Gasteiger charges on atoms. Based on the site-specific markers used in our experiment, we have obtained that coumarins binds specifically to the site 1. Moreover, many studies proposed Sudlow´s site 1 as the binding region for warfarin and bulky heterocyclic compounds (Ghuman et al., 2005). In all dockings, a grid map with 50 × 50 × 50 Å points along the *x*, *y* and *z* axes, and a grid-point spacing of 0.375 Å was applied and the maps were centered on C_α of Trp-214. We used the following GA docking parameters: 30, number of individual in the population: 150, maximum number of energy evaluations: 250 000 and maximum number of generations: 27 000. During docking, a maximum number of 30 conformers was considered, and the root mean square (RMS) cluster tolerance was set to 2 Å. The lowest energy conformations were used as the starting points in the molecular dynamics (MD) simulation.

2.4. Interaction with HSA: molecular dynamics study

MD simulations of the ligand-protein complexes were performed to further investigate ligands binding, and the effect of their structures on the intermolecular interactions. We used the CHARMm force field (Brooks et al., 1983) implemented in the module of Discovery Studio 4.5. The HSA complexes were surrounded by a cubic box of water molecules (TIP3P model (Jorgensen et al., 1983)) extending up to a distance of 12 Å from any solute atom. Additional Na and Cl ions were added randomly to each complex at a concentration of ~0.15 M, close to

physiological conditions (Aqvist, 1990) using the Solvation module of Discovery Studio 4.5. All energy minimization and molecular dynamics simulations were performed using the Particle Mesh Ewald (PME) method (Essmann et al., 1995) for the correct treatment of electrostatic interactions (Sagui and Darden, 1999) and periodic boundary conditions. All initial configurations were optimized by a series of energy minimizations: first only keeping the solvent fixed, second, keeping the protein and coumarin derivative fixed, and finally removing all constraints. The restrains were weak with force constant of 2 kcal/(mol·Å^2). Next, energy minimization was performed using the steepest descent algorithm of 1000 steps, followed by the conjugate gradient algorithm for 1000 steps to reduce unfavorable intermolecular steric contact (until the RMS gradient of the structure was below 0.01 kcal/(mol·Å)). The MD protocol contained a heating step performed for 50 ps with a time step of 1 fs when the system was heated from 50 to 300 K. Prior to the production stage, the system was equilibrated by allowing it to evolve spontaneously until the average temperature and the structure remained stable and the total energy converged. The total number of steps to perform the dynamic simulation was 200 ps. The periodic boundary condition was used and the motion equations were integrated by applying the Leapfrog Verlet algorithm (Verlet, 1967) with a time step of 2 fs. To allow one to keep bonds involving the H atoms at their equilibrium length, the SHAKE algorithm (Ryckaert et al., 1977) was used. The equilibrated system was taken as the starting structure for 5 ns production runs in the NPT ensemble, at a temperature of 300 K maintained using a Berendsen thermostat (Berendsen et al., 1984). The coordinates were recorded every 10 ps. Trajectory structures for analysis were saved at 1 ps.

2.5. Interaction with HSA: binding free enthalpy calculations

The free enthalpy analysis was performed using the MD implementation of the MM-PBSA approach (Kollman et al., 2000), based on the MD trajectories obtained using explicit solvent molecules. The binding free enthalpy (ΔG_{bind}) of coumarin derivatives to HSA was calculated using the following equation:

$$\Delta G_{bind} = G_{HSA\text{-}ligand} - G_{HSA} - G_{ligand} \quad (1)$$

where $G_{HSA\text{-}ligand}$ – free enthalpy of complex, G_{HSA} – free enthalpy of HSA and G_{ligand} – free enthalpy coumarin derivative.

We used 500 snapshots of the solute sampled regularly from the last nanoseconds of the MD trajectories, with the water and counter ions removed. This method combines the enthalpy or molecular mechanics energies (E_{MM}) that represent the internal energies along with van der Waals (E_{vdW}) and electrostatic interactions (E_{elec}), with the solvation free enthalpy (G_{solv}) calculated by the finite difference Poisson-Boltzmann (PB) model for polar solvation (G_{PB} or G_{polar}) and the non-polar contribution ($G_{non\text{-}polar}$) as a function of solvent-accessible surface area (SASA). All terms were computed with the Discovery Studio 4.5 program.

Binding free enthalpy was calculated based on the average structures obtained from the last 3 ns of MD trajectories. The components of each complex were minimized using the conjugate gradient method for 10 000 steps after 100 steps of the steepest descents algorithm and a dielectric constant of 4 for the electrostatic interactions until the RMS gradient of the structure was less than 0.001 kcal/(mol·Å).

3. Experimental section

3.1. Preparation of stock solutions

HSA (as lyophilized powder with fatty acids), NaH_2PO_4, Na_2HPO_4, KOH, HCl and NaCl were obtained from Sigma-Aldrich in *puriss* quality. Doubly distilled Milli-Q water was used for sample preparations. HSA solution was freshly prepared before the experiments and its concentration was estimated from its UV absorption: $\varepsilon_{280\ nm}$(HSA) = 36850 $M^{-1} \cdot cm^{-1}$ (Chasteen et al., 1986). Stock solutions of coumarin derivatives were prepared in water from their hydrochloride salts (pH ~ 4) at 100 μM concentration.

3.2. pH-dependent UV-visible spectrophotometric and spectrofluorometric studies of the ligands

The pH-dependent measurements for the determination of the proton dissociation constants (pK_a) of the compounds **1** – **6** were carried out at 25.0 ± 0.1 °C in aqueous phase at a constant ionic strength of 0.10 M (KCl). The titrations were performed with a carbonate-free KOH solution (0.10 M) and its concentration was determined by pH-potentiometric titrations. pH-Dependent titrations were performed in the pH range 2.0 – 11.5. The initial volume of the samples was 10.0 mL. Samples were deoxygenated by bubbling purified argon through them for ca. 10 min prior the measurements.

The proton dissociation constants and the spectra of the individual species in the various protonation states were calculated with the computer program PSEQUAD (Zékány et al., 1985). The calculations were always made from the experimental titration data measured in the absence of any precipitate in the solution. A Hewlett Packard 8452A diode array spectrophotometer was used to record the UV-visible (UV-vis) spectra in the interval 200 – 800 nm. The path length was 4 cm. The spectrophotometric titrations were performed on samples containing 2.0 μM tested compounds.

The fluorescence spectra of the compounds were recorded at pH 7.4 on a Hitachi-4500 spectrofluorometer with the appropriate excitation wavelength and emission wavelength ranges. The emission spectra were recorded in 1 cm quartz cell at 25.0 ± 0.1 °C using 5 nm/5 nm slit widths. The samples contained 2.5 – 10 μM tested compounds. Three-dimensional spectra were recorded in the 250 – 500 nm excitation and 260 – 600 nm emission wavelength regions at various pH values.

3.3. Interaction with HSA: Spectrofluorometric studies

All samples were prepared in 20 mM phosphate buffer (pH 7.4) and 0.1 M KCl. Samples contained 1 μM HSA and various HSA-to-ligand ratios (from 1:0 to 1:10) were used. Spectra were recorded after 60 min incubations. The excitation wavelength was 295 nm; the emission intensities were read in the range of 310 – 600 nm with 5 nm/5 nm slit widths. The conditional binding constants (logK) were calculated with the computer program PSEQUAD as described in the Supplementary data.

Corrections for self-absorbance and inner filter effect were necessary in the quenching experiments because fluorescence light was significantly absorbed by the coumarin derivatives. The corrections were carried out according to the following equation:

$$F_{corrected} = F_{measured} \cdot 10^{(A_{(EX)} + A_{(EM)})/2} \quad (2)$$

where $F_{corrected}$ and $F_{measured}$ are the corrected and measured fluorescence intensities, and $A_{(EX)}$ and $A_{(EM)}$ are the absorbance values at the excitation and emission wavelengths of the samples, respectively.

4. Results and discussion

4.1. In silico drug likeness and toxicity assessments

Seven principal descriptors and sixteen predicted ADMET properties were calculated for six analyzed coumarin derivatives. Principal descriptors (Lipinski′s rule of five and the topological polar surface area (TPSA) and pK_a values) are given in Table 1. TPSA values of all compounds were found to be between 55.15 and 86.78 Å and lay within the range for a drug with the passive molecular transport through membranes. The values below 90 Å create favorable conditions for the penetration BBB which is important for the ligands interacting with brain receptors. The logP values were within the range 3.83 – 4.81 for the majority of compounds what is in an agreement with the values for well absorbed compounds. For two coumarin derivatives, **1** and **6,** the logP values were predicted to be above 5 indicating even higher lipophilicity. We also examined pH-dependent logD values, which give estimate of the lipophilicity of a drug at the pH of blood plasma. For all compounds the logD values are predicted to be in the 3.77 – 5.01 range, exceeding the traditionally cutoff value of 3.5. The lower lipophilicity value of **4** suggests that it is mostly in the free form and can be distributed to blood cells whereas the higher lipophilicity values of **1** – **3** and **5** – **6** indicates higher probability of binding to plasma proteins (Wils et al., 1994) (Laznicek and Laznickova, 1995). In the study, also specific attention was given to pK_a values. The predicted pK_a values of all compounds fall in the range of 6.60 - 7.45 (see Table 1) and can be attributed to the deprotonation of one of the piperazine nitrogen's ^{+}NH (Fig. S1). The change from butylene to propylene linker slightly decreases the pK_a values. The molecular weights (MWt) of all investigated systems are in the range defined for orally available compounds and only compound **1** has the MWt of more than 500 g/mol, since two chlorine atoms at positions 2 and 3 of the benzene ring increase its MWt to 503.43 g/mol. The number of atoms which can be engaged in the intermolecular hydrogen bonds and the number of rotatable bonds are also within the usually-acceptable ranges.

The predicted drug likeness parameters (volume of distribution (V_d), water solubility (S_w), effective permeability (P_{eff}), apparent permeability (MDCK), BBB_filter, blood-brain barrier partition coefficient (logBB), percentage of unbound drug to blood plasma proteins (%Unbnd), blood-to-plasma concentration ratio (RBP) are shown in Table 2. The volume V_d is the primarily pharmacokinetic parameter which can help in defining the dose required to give a certain plasma concentration. V_d values of six tested compounds are in the range 3.533 – 6.205 L/kg, and they are not distributed in all tissues in the body. Compounds **4** and **6** which have value below 3.7 L/kg are predicted to be confined to the blood plasma, whereas compounds **1**, **2**, **3** and **5** have values higher than 3.7 L/kg, what suggests that they are distributed in whole blood. The aqueous solubility (S_w) significantly affects absorption and distribution characteristics of a compound. The S_w values for all compounds are predicted to be in the 0.00037 – 0.014 mg/mL range and only one system is predicted to have acceptable solubility (4,7-dimethyl-5-[4-(4-(3-methoxyphenyl)piperazin-1-yl)butoxy]coumarin (**6**) – S_w = 0.014 mg/mL). Human jejunal permeability (P_{eff}) reflects the passive transport velocity in cm/s across the epithelial barrier in the human jejunum – the region of the intestinal tract with the largest surface area. The predicted P_{eff} values are in the region 3.581 – 5.137 cm/s·10^4 what show their high jejunal permeability. Madin-Darby Canine Kidney (MDCK) values obtained in the range 624 – 1224 cm/s·10^7 showing good apparent membrane permeability.

The next molecular descriptors (BBB_filter and log BB) determine the likelihood of crossing the BBB. These parameters are crucial in drug design of CNS-active compounds. Both parameters (see Table 2) for six coumarins studied are characteristic for compounds which cross the BBB. The highest concentration in brain is predicted for compound **5** with (2-fluorophenyl)piperazinyl moiety connected via butylene linker. Another important property of a

potential drug is its ability to bind to plasma proteins, which is in most cases considered as undesirable. On the other hand binding to HSA can increase the drug's biological half-life. Two parameters characterize these properties: the percent of drug unbound to protein within blood plasma (%Unbnd) and the concentration of the drug in whole blood compared to plasma (RBP). For the majority of analyzed coumarins the values of %Unbnd are in the region 0 – 1.563%, and the values of RBP in the region 0.62 – 1.38 (see Table 2), what suggests that all compounds fall in the region of high plasma protein binding.

The predicted toxicity parameters for coumarins are shown in Table 3. MRTD is a qualitative assessment of the maximum recommended therapeutic dose administrated with the threshold for dose-related side effects of 3.16 (mg/kg-bw/day). All tested coumarins have MRTD values below 3.16 (mg/kg-bw/day) indicating potential side effects. The hepatotoxicity models, however, predicts all coumarins as "non-toxic". On the other hand six coumarins are also predicted as having potential cardiotoxicity and hERG_pIC_{50} values are in the range between 6.20 and 7.07, exceeding the cutoff value 5.5. It means that these compounds can potentially block hERG channels in the heart cells leading to cardiac problems.

Because the increase of toxicity is forced by the increasing the therapeutic dose, we are taking into account high values of plasma binding of tested coumarins. Our further studies were devoted to the analysis of molecular mechanism of 5-hydroxycoumarin derivatives binding to HSA by experimental measurements and molecular modeling. Analyses of albumin-coumarin interactions can be useful for providing safer and efficient therapy.

4.2. Spectrofluorometric studies of interaction with HSA

The interaction of compounds **1 – 6** with human serum albumin (HSA) has been investigated by fluorescence quenching spectroscopy. HSA is the most abundant plasma protein

(~630 μM) and serves as a transport vehicle for a wide variety of endogenous compounds and pharmaceuticals. The intrinsic fluorescence of HSA is due to aromatic amino acid residues such as tryptophan, tyrosine and phenylalanine (Fanali et al., 2012; Peters, 1996). This protein contains a single tryptophan (Trp-214) residue that is the dominant source of its intrinsic fluorescence, since Trp has much higher quantum yield compared to that of the other two amino acids. Trp-214 is located near to site 1, hydrophobic binding pocket in subdomain IIA. Upon excitation at 295 nm, HSA emits strong fluorescence at 340 nm which can be attenuated by a binding event at, or close to, the Trp-214 due to its high sensitivity to changes in its (local) environment (Fanali et al., 2012; Peters, 1996; Sudlow et al., 1976). Therefore, fluorescence Trp-214 quenching is a simple and indispensable method for monitoring binding at site 1.

Time-dependence measurements on the HSA-compound interaction revealed that the reaction is relatively fast (completed within 20 min), and to ensure the equilibrium state 1 h incubation time was used for the quenching experiments. The self-absorption of the samples is significant at the wavelength range of the quenching measurements; thus a correction equation was applied to minimize this effect. Representative fluorescence emission spectra recorded for the **6** – HSA system at various ratios are shown in Fig. 2, and for **1** – HSA system in Fig. S2. As the studied compounds possess intrinsic fluorescence, their own emission bands are partly overlapped by that of HSA. The overlapping of the spectra of HSA and **3** concerns a too wide wavelength range that hindered the determination of the quenching constant. In the other cases a wavelength range, in which no significant contribution of the compound's emission to the intensity is seen, could be chosen for the calculations (*e.g.* 310 – 360 nm for **6**, see Figs. 2b and 2c). The conditional stability constants (logK) were computed with the computer program PSEQUAD, and are collected in Table 4. It is worth mentioning that the intensities do not tend to

zero intensities at the $\lambda_{(EM)max}$ value of HSA (Fig. 3); and this phenomenon was included in the calculations (see the Supplementary data for the calculations). A possible explanation of this effect can be the partial quenching of Trp-214 emission instead of complete quenching; moreover HSA contains other less emitting residues like Tyr whose emission is not affected by an interaction on site 1.

The changes of the emission intensity of the compounds upon binding to HSA were also analyzed. Fig. 3 shows the intensity of **6** at 452 nm in the absence and in the presence of the protein and only a minor difference can be observed. Similar findings for the other compounds also confirm that the emission intensity of them was insensitive to binding to HSA in our study. Thus no binding constants could be calculated from the side of the compounds, only via the Trp-214 quenching. Representative three-dimensional fluorescence spectra of **3**, HSA and the **3** - HSA system at pH 7.4 (Fig. 4) clearly show that the peak belonging to the HSA is decreased upon binding, while the peak of the compound shows a minor alteration.

In order to compare the quenching ability of the compounds I/I_0 values at the emission maximum (338 nm) are plotted against the HSA-to-ligand ratios (Fig. 5). The fluorescence intensity was slightly increased in the case of **3** due to the overlapping with the emission band of the compound itself (see above). A clear trend is seen here as well as the calculated logK values (Table 4) show the order of the binding strength at site 1 on HSA: **6**, **1** > **4** > **2** > **5**. (Notably, data obtained for **5** was not adequate for the accurate calculations due to the small changes detected.) It could be concluded based on the fluorescence quenching study with HSA that the compounds showed a significant binding on site 1. The determined binding strength (logK = 4.8 – 5.8) is weaker than that of several reduced Schiff base coumarin derivatives studied in our former work (Dömötör et al., 2014). Received dissociation constants ($K_D \sim 1.6 – 16$ μM) were

higher than those obtained before ($K_D \sim 0.03 – 2.09$ μM), however recently tested molecules are smaller and contain a phenolate moiety that plays important role in the binding via electrostatic interactions.

4.3. Site 1 with starting conformations of 5-hydroxycoumarins by molecular docking

The most favorable six conformations of **1** – **6** with the lowest docking energy were found in 30 independent runs. The free energies estimated by intermolecular energy (including van der Waals energy, hydrogen bonding energy and electrostatic energy) were as follows -5.47 kcal/mol (**1**), -5.06 kcal/mol (**2**), -3.34 kcal/mol (**3**), -5.19 kcal/mol (**4**), -4.54 kcal/mol (**5**) and -5.69 kcal/mol (**6**). The conformations corresponding to the lowest energies were selected for MD simulations.

The 3D views of site 1 in HSA are shown in Fig. 6. In Fig. 6a there is a hydrophilic region at the entrance of the pocket (formed by Tyr-150, Lys-195, Lys-199, Arg-218, Leu-219, Arg-222, and Glu-292), and a hydrophobic region at the bottom (formed by Trp-214, Arg-218, Leu-219, Leu-234, Leu-238, His-242, Arg-257, Leu-260, Ala-261, Ile-264, Ile-290, and Ala-291). The predicted location of studied coumarin derivatives in HSA pocket is similar (see Fig. 6b), and their interactions are mainly hydrophobic in nature. The schematic presentation of interactions between coumarin derivatives and HSA is shown in Fig. S3 in Supplementary data. In the best binding poses coumarin derivatives are surrounded by hydrophobic residues and there is a considerable number of hydrogen bonds and electrostatic interactions due to the presence of several hydrophilic amino acids such as Tyr-150, Ser-192, Lys-195, Arg-218, Glu-153, Arg-222, His-242, Arg-257, His-288, Ala-291 and Glu-292 in the vicinity of the ligand. The formation of unfavorable bonds was noticed for all compounds between the proton at the piperazine nitrogen and Lys-199, and for compounds **3**, **4**, **5** additionally with Arg-222.

*4.4. Binding free enthalpy and interactions of 5-hydroxycoumarin derivatives **1** – **6** with HSA*

Finally, the structures of HSA complexes with **1** – **6** were built using MD methodology described in *Section 2.4*. The resulted RMSD values between the ligand starting and average structures were low in all cases. The theoretical binding free enthalpy values were calculated and are shown in Table 5 together with the experimental values obtained using Gibbs´ isotherm and logK values (ΔG_{exp} = -2.303·R·T·logK). The computationally calculated binding free enthalpies and the experimentally obtained values are similar with the maximum difference of 1.23 kcal/mol. The resulting differences may be due to that, the X-ray structure of the protein from crystals even after MD simulation differs from that of aqueous conditions. Compounds **1** – **6** bind to site 1 in different way and with different affinities. The binding affinities decrease in the sequence: **6** > **1** > **4** > **2** > **5** > **3** (-8.26 kcal/mol > -7.04 kcal/mol > -5.75 kcal/mol > -5.31 kcal/mol > -5.75 kcal/mol > -4.09 kcal/mol > -3.03 kcal/mol). The structures of HSA – ligand complexes are shown in Fig. 7 for **1** – **4** and in Fig. 8 for **5** and **6**. Additionally, the location of ligands in respect to Trp-214 was shown in Fig. S4 in Supplementary data.

The coumarin rings of all tested compounds were similarly located within the hydrophobic binding pocket of HSA, while the rest of molecules (composed with alkyl chains, piperazine and benzene rings) decided about the difference in binding modes. Compounds **1**, **3** and **4** with propylene linker are predicted to be accommodated in the HSA pocket in folded conformations, but compound **2** adopted an extended conformation. The coumarin ring of **1** is rotated by 180^{o} when compared with coumarin rings of **2**, **3** and **4**. Compound **1** is surrounded by Tyr-150, Ala-291, His-242 and Glu-292 of HSA forming hydrogen bonds with the ligand, and Lys-195 and Arg-222 creating electrostatic interactions with the 2,3-dichlorophenyl moiety. It can be observed that the methyl group at 7-position makes π-interactions with the indole ring of

Trp-214 (the length of 2.27 Å, Fig. S4). The conformations and locations within the cavity of **3** and **4** are almost the same, but nitrile group of **4** formed a very strong hydrogen bond with Lys-199, which can be responsible for its higher affinity than **3**.

Compounds **5** and **6** with butylene linker are clustered in the center of site 1 of HSA, and in Fig. 8 it can be seen that their conformations are rather different. Coumarin ring in **6** adopts the similar orientation like this of **1**. Apart of typical interactions, folded conformation of **6** allowed for favorable interactions of the 3-methoxyphenyl moiety with Pro-447 and Asp-451 and the water molecule. It is worth noticing that the Trp-214 residue of HSA is near to **6**, forming the hydrophobic interaction similar to that of **1** (Fig. S4). The highest affinity of **6** can be attributed to the folded conformation and may be facilitated by the lack of the acetyl substituent and butylene chain. This hypothesis can be supported by lower affinity of **3**, which is the derivative with both the acetyl group and propylene chain. The **5** – HSA complex showed a similarly extended conformation as the **2** – HSA complex with the 2-fluorophenyl substituent. Fluorophenyl substituents interacted with Glu-292 and Glu-153 in **5**, and with Ser-192, Glu-292 and Lys-195 in **2**. On the basis of theoretical results it can be concluded that all structural features (the substituents, length of alkyl chain) play important role in HSA binding. Compounds **1** and **6** with the highest affinity have almost identical location in Sudlow's site 1 and are in proximity of Trp-214.

4.5. Proton dissociation processes and fluorescence properties of the compounds

The selected compounds have insufficient water solubility, therefore their proton dissociation processes were studied in pure aqueous solution at fairly low concentration (2 μM) by UV-vis spectrophotometry. However, the presence of the coumarin moiety in the compounds results in relatively strong absorption in the UV region. In order to obtain adequately high absorbance

values 4 cm path length had to be applied. Based on the UV-vis spectra recorded at various pH values one deprotonation process was observed in all cases, and pK_a values obtained by the deconvolution of the spectra are collected in Table 4. Representative UV-vis spectra are shown for **6** in Fig. 9a, which reveal relatively minor changes upon deprotonation. The proton dissociation constants can be attributed most probably to the deprotonation of one of the piperazine nitrogen's, namely to the $^{+}NH - CH_2$ moiety as was mentioned in *Section 4.1* and showed in Fig. S1. As this moiety is located relatively far from the chromophore groups (phenyl and coumarin) it is reasonable that the absorption spectra are not so sensitive to the deprotonation.

Figs 9b and 9c represent the decreasing absorbance values for **6** at 306 nm and concentration distribution curves as a function of pH calculated on the basis of the pK_a value. Calculated molar absorbance spectra are shown for selected compounds in Fig. 10, and λ_{max} and molar absorptivity (ε) values for the HL^+ and L forms are collected for all studied compounds in Table 4. It can be concluded that in all cases the $HL^+ \rightarrow L$ process is accompanied by a minor decrease of the λ_{max} values and diminished absorbance of the well-defined band at 286 – 306 nm. The pK_a values calculated based on the experimental data collected in aqueous solution fall in the range of 6.54 – 7.09. It can be seen that the exchange of the butylene linker between the coumarin and piperazine moieties to propylene linker slightly decreases the pK_a values, and the presence of the chlorine substitutes undoubtedly increases the acidity of the compounds due to its high electron withdrawing effect. Interestingly the fluorine monosubstitution resulted in a small increase in the pK_a values. Notably the experimentally obtained pK_a values show a good agreement with the predicted ones (Table 1) in the case of ligands **1** – **3**, although they differ more significantly for **4** – **6**.

Based on the determined pK_a values distribution at pH 7.4 was calculated (Table 4). All the compounds are partly protonated at this pH and 12 – 33% are present in the positively charged HL^+ form. The strongly lipophilic nature of the studied compounds did not allow us to determine the *n*-octanol/water partition coefficients (logP) by the traditional saturation shake flask method (see calculated values *vide supra*). Notably, the protonation of the $N_{piperazine}$–CH_2 moiety enhances the water solubility so much that acidic stock solutions of 100 μM concentration (pH ~ 4) could be prepared for the measurements.

As the studied compounds contain the coumarin moiety, their fluorescence activity is expected. Therefore fluorescence properties were studied and the $\lambda_{(EM)max}$ values are collected in Table 4. It was found that in spite of the close structural similarities of the compounds their fluorescence property was quite different depending on the nature and position of the substituents. Although the $\lambda_{(EM)max}$ values are similar (439 – 445 nm), their fluorescence intensities considerably differ (Table 4). The compound **6** was found to be the strongest emitting compound, while fluorescence of **1** is almost negligible.

5. Conclusions

Drug likeness characteristics computed for six coumarins with strong binding ability towards 5-HT_{1A} and 5-HT_{2A} receptors allowed for evaluation of their drug potency. TPSA values of all compounds were found within range 55.15 – 86.78 Å what means that they capable of the penetration of the BBB what is important for the potential ligand of brain receptors. Theoretical values of the percent of drug unbound to protein within blood plasma (%Unbnd) were in the range 0 – 1.6 % suggesting that tested coumarins are characterized by a significant plasma protein binding. Examinations of coumarin derivatives affinities to HSA by fluorescence

quenching spectroscopy revealed moderate binding of coumarins **1** – **6,** suggesting a specific role of HSA as a carrier molecule of coumarins with piperazine moiety. The experimental data were in good agreement with the computationally-derived free enthalpies of binding obtained by MD ligand docking in Sudlow´s site 1. *In-silico* analysis of the interactions of coumarin derivatives with HSA shed more light onto the interpretation of mode of action of investigated coumarins which can be mainly characterized as the hydrophobic and hydrogen bonding types. Experimentally determined acidity constants (pK_a) allowed the determination of distribution of ligands in the various protonated forms at pH 7.4. It showed that 12 – 33% of compounds are present in their positively charged HL^+ form, in which the piperazine nitrogen is protonated. On the basis of received results the tested coumarins could be considered as promising compounds for further development steps as novel therapeutic agents.

Authorship contributions

The manuscript was written through contributions of all authors. All authors have given approval to the final version of the manuscript.

Acknowledgement

The results presented in this work were obtained using the resources of Interdisciplinary Center for Mathematical and Computational Modeling (ICM) Warsaw University (G26-10). This work was supported by the Hungarian National Research, Development and Innovation Office-NKFI through project FK 124240, and the UNKP-17-4 (E.A.E.) and UNKP-17-2 (V.P.) New National Excellence Program of the Ministry of Human Capacities.

References

Abdelhafez, O.M., Amin, K.M., Batran, R.Z., Maher, T.J., Nada, S.A., Sethumadhavan, S., 2010. Synthesis, anticoagulant and PIVKA-II induced by new 4-hydroxycoumarin derivatives. Bioorg. Med. Chem. 18, 3371-3378.

Ahmed-Ouameur, A., Diamantoglou, S., Sedaghat-Herati, M.R., Nafisi, S., Carpentier, R., Tajmir-Riahi, H.A., 2006. The effects of drug complexation on the stability and conformation of human serum albumin: protein unfolding. Cell Biochem. Biophys. 45, 203-213.

Aqvist, J., 1990. Ion water interaction potentials derived from free-energy perturbation simulations. J. Phys. Chem.-Us 94, 8021-8024.

Bailey, D.N., Briggs, J.R., 2004. The binding of selected therapeutic drugs to human serum alpha-1 acid glycoprotein and human serum albumin *in vitro*. Ther. Drug Monit. 26 (1), 40 - 43.

Berendsen, H.J.C., Postma, J.P.M., van Gunsteren, W.F., DiNola, A., Haak, J.R., 1984. Molecular dynamics with coupling to an external bath. J. Chem. Phys. 81, 3684-3690.

Bertucci, C., Domenici, E., 2002. Reversible and covalent binding of drugs to human serum albumin: methodological approaches an physiological relevance. Curr. Med. Chem. 9, 1463 - 1481.

Bhattacharya, A.A., Grune, T., Curry, S., 2000. Crystalographic analysis reveals common modes of binding of medium and low-chain fatty acids to human serum albumin. J. Mol. Biol. 303, 721-732.

Biovia Software Inc., Discovery Studio Molecular Environment, Release 4.5, San Diego: Biovia Software Inc., 2015.

Breneman, C.M., Wiberg, K.B., 1990. Determing atom-centered monopoles from molecular electrostatic potentials. The need for high sampling in formamide conformational analysis. J. Comput. Chem. 11, 361-373.

Brooks, B.R., Bruccoleri, R.E., Olafson, B.D., States, D.J., Swaminathan, S., Karplus, M., 1983. Charmm - a program for macromolecular energy, minimization, and dynamics calculations. J. Comput. Chem. 4, 187-217.

Carter, D.C., Xo, J.X., 1994. Structure of serum albumin. Adv. Protein Chem. 45, 153-176.

Chasteen, N.D., Grady, J.K., Holloway, C.E., 1986. Characterization of the binding, kinetics, and redox stability of vanadium(IV) and vanadium(V) protein complexes in serum. Inorg. Chem. 25, 2754-2760.

Chen, Y., Lan, Y., Wang, S.L., Zhang, H., Xu, X.Q., Liu, X., Yu, M.Q., Liu, B.F., Zhang, G.S., 2014. Synthesis and evaluation of new coumarin derivatives as potential atypical antipsychotics. Eur. J. Med. Chem. 74, 427-439.

Chen, Y., Wang, S., Xu, X., Liu, X., Yu, M., Zhao, S., Liu, S., Qiu, Y., Zhang, T., Liu, B.-F., Zhang, G., 2013. Synthesis and biological investigation of coumarin piperazine (piperidine) derivatives as potential multireceptor atypical antipsychotics. J. Med. Chem. 56, 4671-4690.

Curry, S., 2009. Lessons from the crystallographic analysis of small molecule binding to human serum albumin. Drug Metab. Pharmacokinet. 24, 342-357.

Dömötör, O., Tuccinardi, T., Karcz, D., Walsh, M., Creaven, B.S., Enyedy, É.A., 2014. Interaction of anticancer reduced Schiff base coumarin derivatives with human serum albumin investigated by fluorescence quenching and molecular modeling. Bioorg. Chem. 52, 16-23.

Drzewiecka, A., Koziol, A.E., Struga, M., Ruizd, T.P., Gomez, M.F., Lis, T., 2013. Structural characterization of derivatives of 4-methylcoumarin – Theoretical and experimental studies. J. Mol. Struct. 1043, 109-115.

Essmann, U., Perera, L., Berkowitz, M.L., Darden, T., Lee, H., Pedersen, L.G., 1995. A smooth Particle Mesh Ewald method. J. Chem. Phys. 103, 8577-8593.

Fanali, G., di Masi, A., Trezza, V., Marino, M., Fasano, M., Ascenzi, P., 2012. Human serum albumin: from bench to bedside. Mol. Aspects Med. 33, 209-290.

Flarakos, J., Morand, K.L., Vouros, P., 2005. High-throughput solutionbased medicinal library screening against human serum albumin. Anal. Chem. 77, 1345-1353.

Frish, M.J., Trucks, G.W., Schlegel, H.B., Scuseria, G.E., Robb, M.A., Cheeseman, J.R., Zakrzewski, V.G., Montgomery, J.A.J., Stratmann, R.E., Burant, J.C., Dapprich, S., Millam, J.M., Daniels, A.D., Kudin, K.N., Strain, M.C., Farkas, O., Tomasi, J., Barone, V., Cossi, M., Cammi, R., Mennucci, B., Pomelli, C., Adamo, C., Clifford, S., Ochterski, J., Petersson, G.A., Ayala, P.Y., Cui, Q., Morokuma, K., Malick, D.K., Rabuck, A.D., Raghavachari, K., Foresman, J.B., Cioslowski, J., Ortiz, J.V., Baboul, A.G., Stefanov, B.B., Liu, G., Liashenko, A., Piskorz, P., Komaromi, I., Gomperts, R., Martin, R.L., Fox, D.J., Keith, T., Al-Laham, M.A., Peng, C.Y., Nanayakkara, A., Gonzalez, C., Challacombe, M.P., Gill, P.M.W., Johnson, B., Chen, W., Wong, M.W., Andres, J.L., Gonzalez, C., Head-Gordon, M., Replogle, E.S., Pople, J.A., 2009. Gaussian, Inc., Pittsburgh, PA.

Garg, A., Manidhar, D.M., Gokara, M., Malleda, C., Reddy, C.S., Subramanyam, R., 2013. Elucidation of the binding mechanism of coumarin derivatives with human serum albumin. Plos One 8.

Ghuman, J., Zunszain, P.A., Petitpas, I., Bhattacharya, A.A., Otagiri, M., Curry, S., 2005. Structural basis of the drug-binding specificity of human serum albumin. J. Mol. Biol. 353, 38-52.

Gokara, M., Sudhamalla, B., Amooru, D.G., Subramanyam, R., 2010. Molecular interaction studies of trimethoxy flavone with Human Serum Albumin. Plos One 5.

Hassan, M.Z., Osman, H., Ali, M.A., Ahsan, M.J., 2016. Therapeutic potential of coumarins as antiviral agents. Eur. J. Med. Chem. 123, 236-255.

Hogson, J., 2001. ADMET – turning chemicals into drugs. Nat. Biotechnol. 19, 722-726.

Il'ichev, Y.V., Perry, J.L., Ruker, F., Dockal, M., Simon, J.D., 2002. Interaction of ochratoxin A with human serum albumin. Binding sites localized by competitive interactions with the native protein and its recombinant fragments. Chem Biol Interact 141, 275-293.

Jorgensen, W.L., Chandrasekhar, J., Madura, J.D., Impey, R.W., Klein, M.L., 1983. Comparison of simple potential functions for simulating liquid water. J. Chem. Phys. 79, 926-935.

Kollman, P.A., Massova, I., Reyes, C., Kuhn, B., Huo, S., Chong, L., Lee, M., Lee, T., Duan, Y., Wang, W., Donini, O., Cieplak, P., Srinivasan, J., Case, D.A., Cheatham, T.E., 3rd, 2000. Calculating structures and free energies of complex molecules: combining molecular mechanics and continuum models. Acc. Chem. Res. 33, 889-897.

Kratochwil, N.A., Huber, W., Muller, F., Kansy, M., Gerber, P.R., 2002. Predicting plasma protein binding of drugs: a new approach. Biochem. Pharmacol. 64, 1355-1374.

Lameh, J., Burstein, E.S., Taylor, E., Weiner, D.M., Vanover, K.E., Bonhaus, D.W., 2007. Pharmacology of N-desmethylclozapine. Pharmacol. Ther. 115, 223-231.

Laznicek, M., Laznickova, A., 1995. The effect of lipophilicity on the protein binding and blood cell uptake of some acidic drugs. J. Pharm. Biomed. Analys. 823-828.

Morris, G.M., Goodsell, D.S., Halliday, R.S., Huey, R., Hart, W.E., Belew, R.K., Olson, A.J., 1998. Automated docking using a Lamarckian genetic algorithm and an empirical binding free energy function. J. Comput. Chem. 19, 1639-1662.

Morris, G.M., Goodsell, D.S., Huey, R., Olson, A.J., 1996. Distributed automated docking of flexible ligands to proteins: parallel applications of AutoDock 2.4. J. Comput. Aided. Mol. Des. 10, 293-304.

Morris, G.M., Huey, R., Lindstrom, W., Sanner, M.F., Belew, R.K., Goodsell, D.S., Olson, A.J., 2009. AutoDock4 and AutoDockTools4: Automated docking with selective receptor flexibility. J. Comput. Chem. 30, 2785-2791.

Ostrowska, K., Grzeszczuk, D., Głuch-Lutwin, M., Gryboś, A., Siwek, A., Dobrzycki, Ł., Trzaskowski, B., 2017. Development of selective agents targeting serotonin $5HT_{1A}$ receptors with subnanomolar activities based on a coumarin core. Med.Chem.Commun. 8, 1690-1696.

Paul, K., Bindal, S., Luxami, V., 2013. Synthesis of new conjugated coumarin-benzimidazole hybrids and their anticancer activity. Bioorg. Med. Chem. Lett. 23, 3667-3672.

Pérez-Ruiz, R., Bueno, C.J., Jiménez, M.C., Miranda, M.A., 2010. In situ transient absorption spectroscopy to assess competition between serum albumin and alpha-1-acid glycoprotein for drug transport. J. Phys. Chem. Lett. 1, 829-833.

Peters, T.J., 1996. All about albumin, biochemistry, genetics, and medical applications. New York: Academic Press.

Petitpas, I., Grune, T., Bhattacharya, A.A., Curry, S., 2001. Crystal structures of human serum albumin complexed with monounsaturated and polyunsaturated fatty acids. J. Mol. Biol. 314, 955-960.

Petitpas, I., Petersen, C.E., Ha, C.E., Bhattacharya, A.A., Zunszain, P.A., Ghuman, J., Nadhipuram, V.B., Stephen, C., 2003. Structural basis of albumin–thyroxine interactions and familial dysalbuminemic hyperthyroxinemia. Proc. Natl. Acad. Sci. USA 100, 6440-6445.

Ryan, A.J., Ghuman, J., Zunszain, P.A., Chung, C.W., Curry, S., 2011. Structural basis of binding of fluorescent, site-specific dansylated amino acids to human serum albumin. J. Struct. Biol. 174, 84-91.

Ryckaert, J.P., Ciccotti, G., Berendsen, H.J.C., 1977. Numerical-integration of cartesian equations of motion of a system with constraints - molecular-dynamics of N-alkanes. J. Comput. Phys. 23, 327-341.

Sagui, C., Darden, T.A., 1999. Molecular dynamics simulations of biomolecules: long-range electrostatic effects. Annu. Rev. Biophys. Biomol. Struct. 28, 155-179.

Sarkanj, B., Molnar, M., Cacic, M., Gille, L., 2013. 4-Methyl-7-hydroxycoumarin antifungal and antioxidant activity enhancement by substitution with thiosemicarbazide and thiazolidinone moieties. Food Chem. 139, 488-495.

Simulations Plus Inc., ADMET Predictor^{TM} Lancaster, California,USA, 2016.

Sitkoff, D., Sharp, K.A., Honig, B., 1994. Correlating solvation free energies and surface tensions of hydrocarbon solutes. Biophys. Chem. 51, 397-403; discussion 404-399.

Skalicka-Wozniak, K., Orhan, I.E., Cordell, G.A., Nabavi, S.M., Budzynska, B., 2016. Implication of coumarins towards central nervous system disorders. Pharmacol. Res. 103, 188-203.

Sudlow, G., Birkett, D.J., Wade, D.N., 1976. Further characterization of specific drug binding-sites on human serum albumin. Mol. Pharmacol. 12, 1052-1061.

Tsay, S.C., Hwu, J.R., Singha, R., Huang, W.C., Chang, Y.H., Hsu, M.H., Shieh, F.K., Lin, C.C., Hwang, K.C., Horng, J.C., De Clercq, E., Vliegen, I., Neyts, J., 2013. Coumarins hinged directly on benzimidazoles and their ribofuranosides to inhibit hepatitis C virus. Eur. J. Med. Chem. 63, 290-298.

Varshney, A., Sen, P., Ahmad, E., Rehan, M., Subbarao, N., Khan, R.H., 2010. Ligand binding strategies of human serum albumin: How can the cargo be utilized? Chirality 22, 77-87.

Verlet, L., 1967. Computer experiments on classical fluids .I. Thermodynamical properties of Lennard-Jones molecules. Phys. Rev. 159, 98.

Wils, P., Warnery, A., Phung-Ba, V., Legrain, S., Scherman, D., 1994. High lipophilicity decreases drug transport across intestinal epithelial cells. J. Pharmacol. Exp. Ther. 269, 654-658.

Yeggoni, D.P., Gokara, M., Manidhar, D.M., Racharnallu, A., Nakka, S., Reddy, C.S., Subramanyam, R., 2014. Binding and molecular dynamics studies of 7-hydroxycoumarin derivatives with human serum albumin and its pharmacological importance. Mol. Pharmaceut. 11, 1117-1131.

Zékány, L., Nagypál, I.i., Leggett, D.L.E., 1985. Computational methods for the determination of formation constants. Plenum Press, New York, pp. 291-353.

Figure and Table legends

Fig. 1. Chemical structures of the coumarin derivatives studied.

Fig. 2. Fluorescence emission spectra of **6** – HSA system (a, b), and **6** alone (c) at various concentrations. (c_{HSA} = 1 μM; $c_{\mathbf{6}}$ = 0-10 μM; λ_{EX} = 295 nm; t = 25 °C; pH = 7.40 (20 mM phosphate buffer); I = 0.1 M (KCl)).

Fig. 3. Fluorescence emission intensities recorded for the **6 –** HSA system at various ratios at 338 nm (□) and at 452 nm (■). The grey dotted line shows the independent calibration for **6**. (c_{HSA} = 1 μM; $c_{\mathbf{6}}$ = 0-10 μM; λ_{EX} = 295 nm; t = 25 °C; pH = 7.40 (20 mM phosphate buffer); I = 0.1 M (KCl)).

Fig. 4. Three-dimensional fluorescence spectra of compound **3** (a) HSA (b) and HSA **– 3** (1:4.5) system (c) (c_{HSA} = 1 μM; $c_{\mathbf{3}}$ = 4.5 μM; t = 25 °C; pH = 7.40 (20 mM phosphate buffer); I = 0.1 M (KCl)).

Fig. 5. Measured quenching of the Trp fluorescence emission intensity of HSA as I/I_0 (%) by the addition of **6** (□), **3** (×); **5** (♦); **2** (Δ); **1** (+); **4** (●). (c_{HSA} = 1 μM; λ_{EX} = 295 nm, λ_{EM} = 338 nm; t = 25 °C; pH = 7.4 (20 mM phosphate buffer); I = 0.1 M (KCl)).

Fig. 6. Views of coumarin derivatives in site 1 of HSA. (a) The hydrophobic and hydrophilic amino acid residues surrounding the ligands. Surface hydrophobicity was depicted by the shaded colors: brown - the hydrophobic and blue - the lipophilic regions. (b) Superposition of compounds: **1** (green), **2** (blue), **3** (orange), **4** (red), **5** (pink), **6** (dark blue).

Fig. 7. Structures of the **1**-HSA, **2**-HSA, **3**-HSA and **4**-HSA complexes, and 2D view of all HSA residues interacting with the ligands resulting from MD simulations (residues involved in

hydrogen bonding marked as green and cyan circles; in hydrophobic interactions marked as pink circle and electrostatic interactions marked as orange circle).

Fig. 8. Structures of the **5**-HSA and **6**-HSA complexes, and 2D view of all HSA residues interacting with the ligands resulting from MD simulation (residues involved in hydrogen bonding marked as green and cyan circles; in hydrophobic interactions marked as pink circle and electrostatic interactions marked as orange circle).

Fig. 9. pH-dependent UV-vis spectra of **6** (a), measured (×) and fitted (solid line) absorbance values at 306 nm as a function of pH (b), and concentration distribution curves (c). (c = 1.98 μM; l = 4 cm; t = 25 °C; I = 0.1 M (KCl)).

Fig. 10. Calculated molar absorbance spectra for ligand species of **2** (black lines), **5** (grey lines) (a); and **4** (black lines), **1** (grey lines) (b) obtained by the deconvolution of the UV-vis spectra recorded at various pH values. (t = 25 °C; I = 0.1 M (KCl)).

Table 1. The topological polar surface area (TPSA), parameters of Lipinski´s rule of five, and predicted proton dissociation constants (pK_a) for coumarins **1** – **6**.

Table 2. Theoretical values of water solubility S_w, effective permeability P_{eff}, apparent permeability MDCK, percentage of unbound drug to blood plasma proteins %Unbnd, blood-to-plasma concentration ratio RBP, BBB filter, blood-brain barrier partition coefficient logBB for coumarins **1** – **6**.

Table 3. Predicted toxicity parameters for coumarins **1** – **6**: maximum recommended therapeutic dose MRTD, level of alkaline phosphatase (AlkPhos); level of γ-glutamyl transferase (GGT), level of serum glutamate oxaloacetate transaminase (SGOT), level of serum glutamate pyruvate

transaminate (SGPT), level of lactate dehydrogenase (LDH); cardiotoxicity – hERG_filter and affinity for hERG K^+ (hERG_pIC_{50}).

Table 4. Proton dissociation constants (pK_a) of for coumarins **1** – **6** determined by UV-vis spectrophotometric titrations, distribution at pH 7.4 and λ_{max}, ε values of the ligand species; $\lambda(EM)_{max}$ and relative fluorescence emission intensity values for the compounds at pH 7.4; conditional binding constants to HSA on site 1 (logK) (t = 25°C).

Table 5. Theoretical and experimental free enthalpies of binding to HSA, and theoretical average distance of ligand to tryptophan Trp-214 for coumarins **1** – **6**.

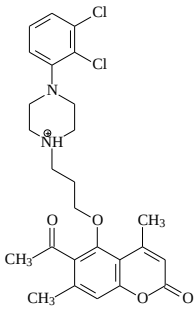

1

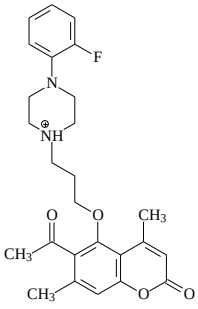

2

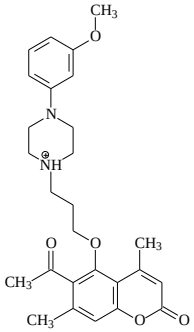

3

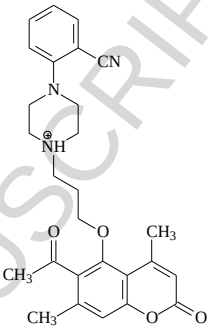

4

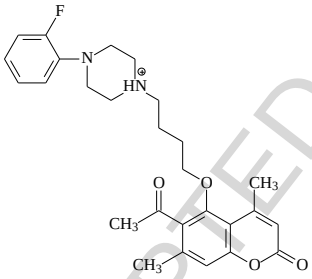

5

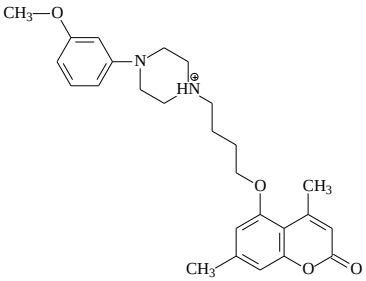

6

Fig. 1.

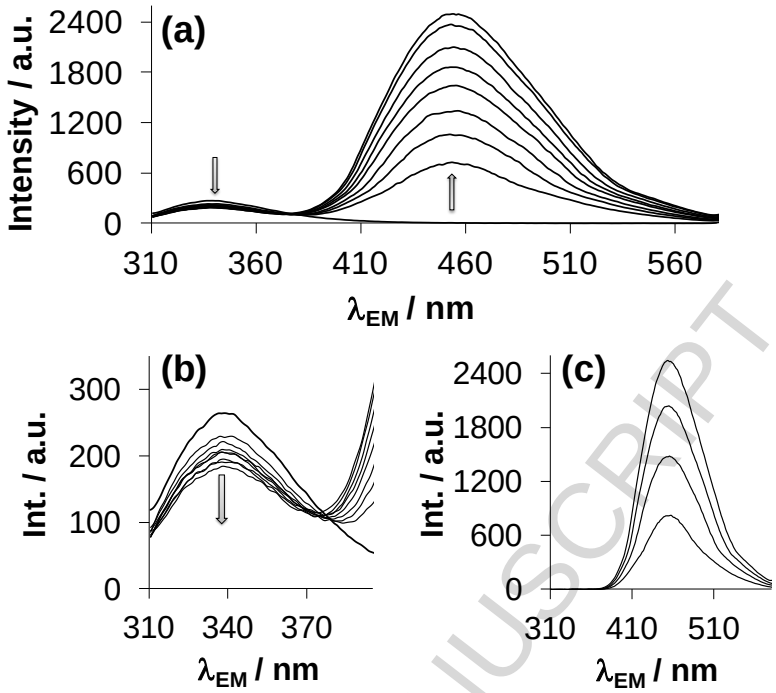

Fig. 2.

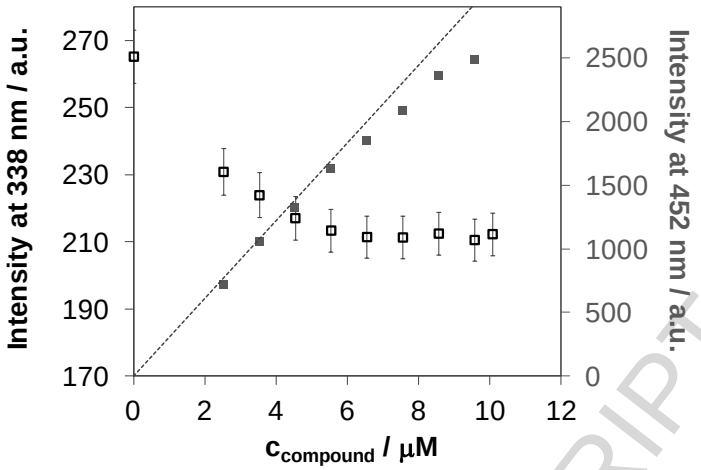

Fig. 3.

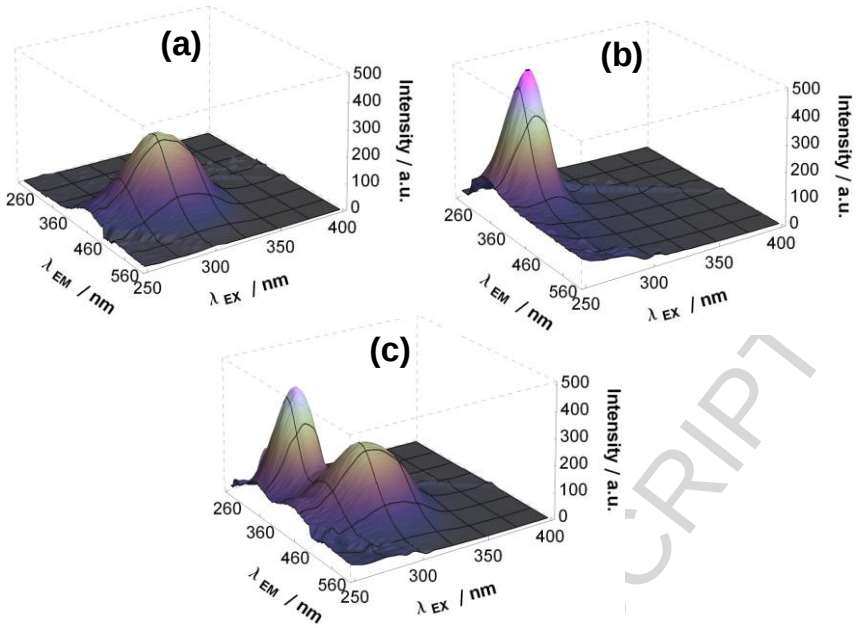

Fig. 4.

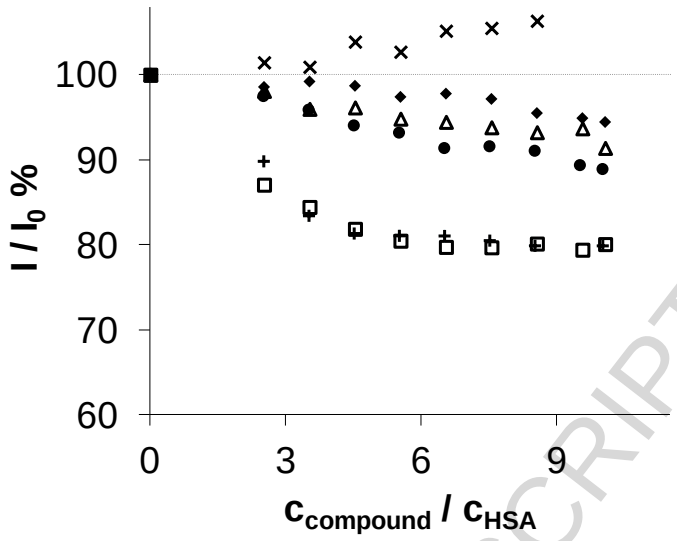

Fig. 5.

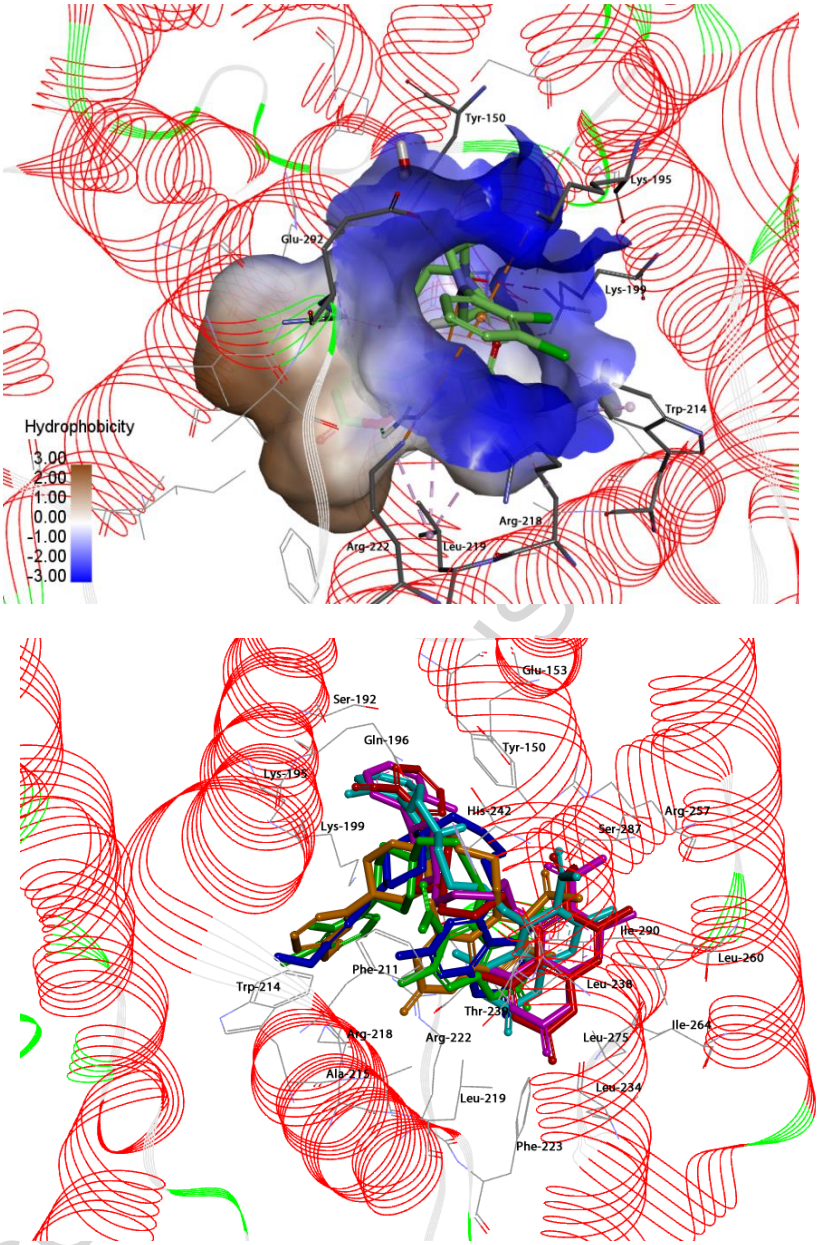

Fig. 6.

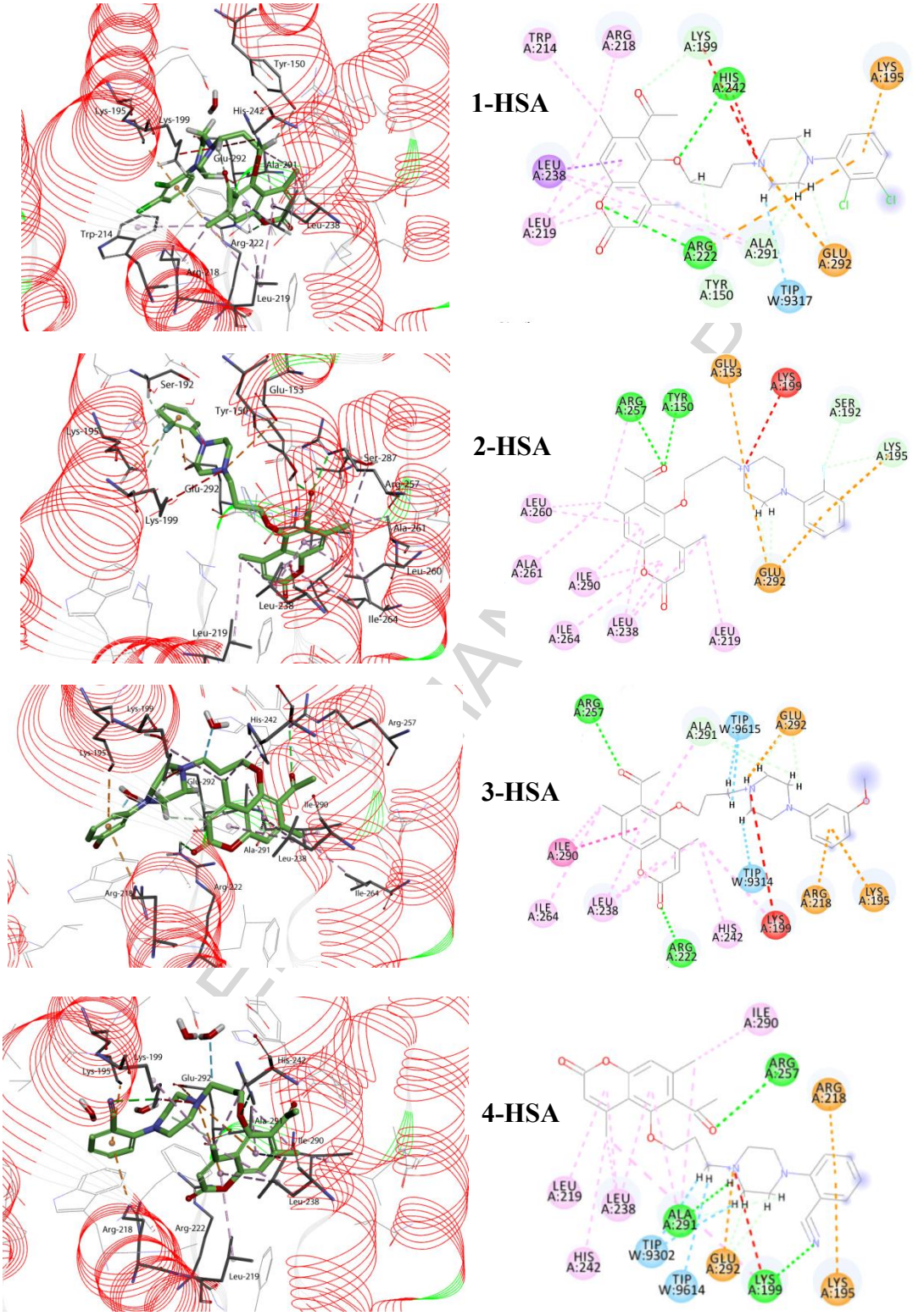

Fig. 7.

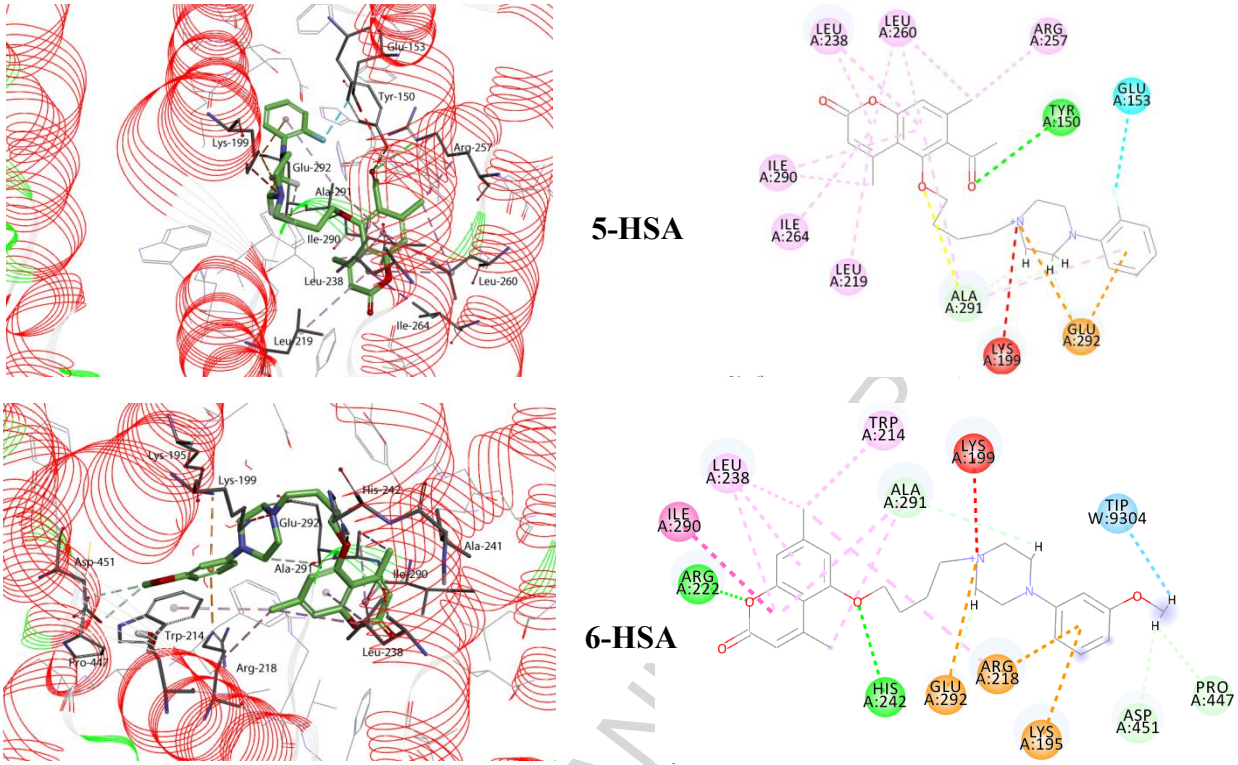

Fig. 8.

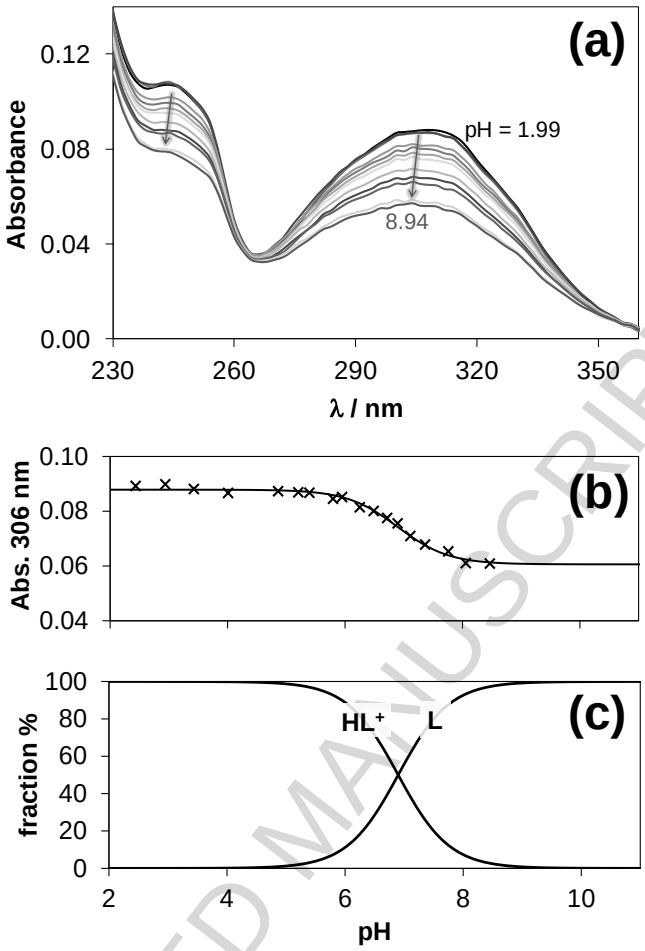

Fig. 9.

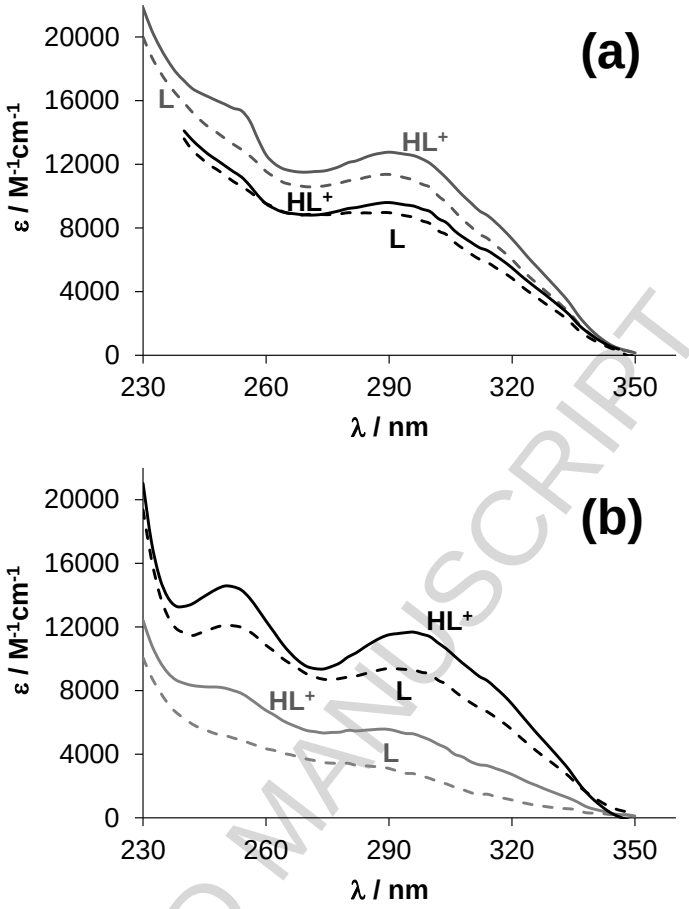

Fig. 10.

Table 1.

Compound	TPSA	MWt	LogP	LogD	HBD	HBA	pK_a
	expected values						
	(<140Å^2)	(≤500 g/mol)	(≤5)	(≤3.5)	(≤5)	(≤8)	
1	62.99	503.43	5.12	5.01	0	6	6.86
2	62.99	452.53	4.50	4.36	0	6	6.98
3	72.22	464.57	4.30	4.21	0	7	6.79
4	86.78	459.55	3.83	3.77	0	7	6.60
5	62.99	466.56	4.81	4.48	0	6	7.45
6	55.15	436.56	5.11	4.81	0	6	7.39

Table 2.

Compound	V_d	S_w	P_{eff}	MDCK	%Unbnd	RBP	BBB filter	logBB
	expected values							
	(≤ 3.7 L/kg)	(≥0.010 mg/mL)	(≥ 0.5 cm/s·10^4)	(≥ 30 cm/s·10^7)	(>10%)	(<1)	(high/ low)	
1	4.622	0.001	5.137	1223.743	0.632	0.684	high	0.275
2	4.551	0.003	4.482	706.579	1.115	0.669	high	0.215
3	3.745	0.005	3.664	655.131	1.268	0.638	high	-0.158
4	3.533	0.00037	4.264	715.301	1.563	0.621	high	-0.576
5	6.205	0.007	3.581	648.081	1.379	0.662	high	0.323
6	3.596	0.014	3.797	624.053	1.020	0.646	high	0.022

Table 3.

Compound	MRDT	hERG filter	hERG pIC_{50}	AlkPhos	GGT	LDH	SGOT	SGPT
	expected values							
	(>3.16 mg/kg/dzień)	(Yes/No)	(>5.5)					
1	Below_3.16	Yes	6.74	NT	NT	NT	NT	NT
2	Below_3.16	Yes	6.41	NT	NT	NT	NT	NT
3	Below_3.16	Yes	7.07	NT	NT	NT	NT	NT
4	Below_3.16	Yes	6.69	NT	NT	NT	NT	NT
5	Below_3.16	Yes	6.20	NT	NT	NT	NT	NT
6	Below_3.16	Yes	6.77	NT	NT	NT	NT	NT

Table 4.

	1	**2**	**3**	**4**	**5**	**6**
pK_a UV-vis[a]	6.54 ± 0.01	6.94 ± 0.04	6.68 ± 0.05	7.09 ± 0.02	7.09 ± 0.02	6.90 ± 0.01
$HL^+_{7.4}$ (%)	12	26	16	33	33	24
$L_{7.4}$ (%)	88	74	84	67	67	76
λ_{max} (nm) /ε ($M^{-1}cm^{-1}$) of HL^+	288(5580) 248(8150)	290(9600)	286(16925) 244(21250)	294(11640) 250(14575)	290(12760) 254(15360)	306(11090) 244(13690)
λ_{max} (nm) /ε ($M^{-1}cm^{-1}$) of L	-	288(8965)	284(16130) 246(21140)	292(9390) 252(12075)	290(11360)	304(7650) 246(1060)
$\lambda(EM)_{max}$ (nm)	445	445	443	439	445	452
relative intensity[b]	0.004	0.124	0.128	0.095	0.329	1.000
logK (HSA)[c]	5.8 ± 0.1	4.8 ± 0.1	n.d.	4.9 ± 0.1	< 4.8	5.8 ± 0.1
K_D[d]	1.6 μM	16 μM	n.d.	13 μM	>16 μM	1.6 μM

[a]I = 0.1 M (KCl), values determined in aqueous phase; [b]Relative fluorescence intensities measured at emission maxima at pH 7.4; [c]Measured at pH 7.4 (20 mM phosphate buffer); [d]K_D = dissociation constants of the HSA adducts (K_D = 1/ K).

Table 5.

Compounds	ΔG_{bind} (kcal/mol)	ΔG_{exp} [a] (kcal/mol)	r (Å)
1	-7.04	-7.904	6.42
			2.27 (π-π)
2	-5.31	-6.541	7.58
3	-3.03	-[*]	8.01
4	-5.75	-6.678	6.04
5	-4.09	< -6.541	5.81
6	-8.26	-7.904	6.39
			4.84 (π-π)

[a] $\Delta G_{exp} = -2.303 \cdot R \cdot T \cdot \log K$

[*] overlapping quenching activity

Graphical abstract